CHAPTER 2

ENTROPY OPTIMIZED MHD FLUID FLOW OVER A VERTICAL STRETCHING SHEET

Content of this chapter is published in:

Heat Transfer (Wiley) 2022 Volume 51(3) 2546-2564 **(Scopus)**

Chapter 2

Entropy optimized MHD fluid flow over a vertical stretching sheet

Entropy optimization is used to enhance the system performance. Entropy generation is caused due to heat fluxes, Joule heating and dissipation etc. To increase the productivity of the systems, The entropy optimization of the system need to be decreased. MHD fluid flow research is important because it has numerous engineering applications, including slurry flows, industrial oils and diluted polymer solutions.

2.1 Introduction of the Problem

The best way to improve system performance is to optimize entropy. The entropy generation affects heat flows, joule heating, mass flux, etc. Entropical system optimization has more chance of irreversibility and thus reduces the system's competence. To create good production systems, we reduce the entropy optimization of our system. Never reduces the unsustainability of the isolated system but in the non-isolated system it is lowered. The second legislation on thermodynamics offers systemic equipment and entropy for reducing resistance. The role of only a few electronic devices helps promote and enhance engineering. The first mention of entropy control was made by Bejan [4, 5].

Magnetohydrodynamics (MHD) is the investigation of attractive property of electrically conducting liquid. MHD has wide applications in various regions like atomic reactors, MHD Generator, and so forth. Turkyilmazoglu [92, 94] investigated consistent MHD laminar flow on a radially contracting and extending rotating plate. Afsana et al. [113] probed a 2D MHD fluid to learn the attributes of heat transfer and entropy production using finite volume process. Arifuzzaman et al. [114] have explained the influence of radiation on natural convective MHD fluid flow. Impact of heat generation on MHD fluid through porous media has been perceived by Kataria

and Patel [42, 43]. Usman et al. [95] explored natural convection flow of MHD fluid under radiation effects. Mathematical modelling for MHD fluid with radiation and heat generation explained by Mittal and Patel [16]. Sheikholeslami et al. [88] examined impact of thermal radiation on MHD fluid flow between two horizontal parallel plates. Electrically conducting fluid flow past over vertical plate in the existance of heat generation scrutinized by Sheikholeslami et al. [89]. Kataria et al. [44] explained impact of magnetic field on MHD fluid flow. Nayak et al. [80] scrutinized effect of magnetic field on incompressible fluid flow over a stretching sheet. Entropy optimized MHD fluid flow have been analysed by Nagaraju et al. [36]. Rashidi et al. [84] considered entropy optimization of steady MHD fluid flow. Reddy et al. [37] explored the influence of viscous dissipation on an electrically conductive MHD fluid over vertical plate.

Many numerical techniques have been developed to obtain the accurate solution. But, due to some restrictions, scientists have considered analytical approaches as an alternative. Among these analytical methods, Homotopy analysis method (HAM) proposed by Liao [120] is one of the most efficient methods to obtain series solutions of the different type of strongly nonlinear equations such as coupled, decoupled, homogeneous and non-homogeneous, which can provide us with a simple way to ensure the convergence of solution series and provide better results compared with other similar methods.

2.2 Novelty of the chapter

Purpose of this chapter is to investigate solution of radiation effect on Entropy optimized MHD fluid flow. Such study may find application in thermal energy, cooling of modern electronic systems, geothermal energy systems, and solar power collectors etc.

2.3 Mathematical Formulation of the Problem

Consider steady, laminar, 2D natural convective flow of an electrically conducting, incompressible, MHD fluid past a verticle stretching surface in the existance of velocity slip. Ignoring magnetic Reynolds number and induced magnetic field. Joule heating, viscous dissipation, heat generation/absorption and thermal radiation are taken into account. physical attributes of irreversibility are discussed. Convective boundary conditions put on the boundary. In Figure 2.1, stretching sheet velocity in the direction of x is $U_w(x) = ax$, with initial stretching rate $a > 0$. Magnetic field

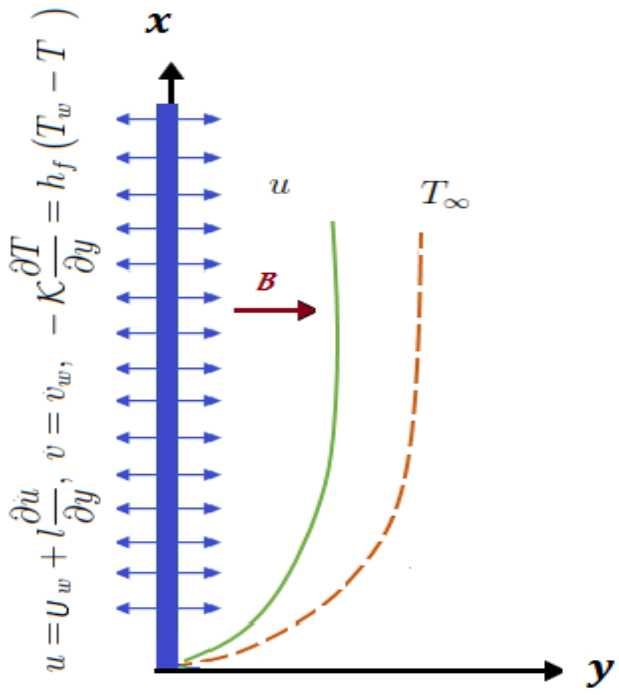

Figure 2.1: Physical sketch

$\mathcal{B} = B_0$ is applied in the perpendicular direction of the flow. The equations which are governed for all these assumptions, are derived using Boussinesq's approximation. They are as follows. The flow expression satisfies

$$\frac{\partial u}{\partial x} + \frac{\partial v}{\partial y} = 0, \tag{2.3.1}$$

$$u\frac{\partial u}{\partial x} + v\frac{\partial u}{\partial y} = \nu\frac{\partial^2 u}{\partial y^2} - \frac{\sigma B_0^2}{\rho}u + g\beta_T(T - T_\infty), \tag{2.3.2}$$

$$\rho C_p\left(u\frac{\partial T}{\partial x} + v\frac{\partial T}{\partial y}\right) = \kappa\frac{\partial^2 T}{\partial y^2} + \mu\left(\frac{\partial u}{\partial y}\right)^2 + \sigma B_0^2 u^2 + Q^*\left(T - T_\infty\right) - \frac{\partial q_r}{\partial y}, \tag{2.3.3}$$

with boundary conditions

$$u = U_w + l\frac{\partial u}{\partial y},\ v = v_w,\ -\kappa\frac{\partial T}{\partial y} = h_f\left(T_w - T\right) \quad \text{at} \quad y = 0. \tag{2.3.4}$$

$$u \to 0,\ T \to T_\infty \quad \text{as} \quad y \to \infty. \tag{2.3.5}$$

In formulating momentum equation (2.3.2), the ratio of thermal diffusivity to magnetic diffusivity has been kept small when compared to unity. In formulating heat equation (2.3.3), Viscous dissipation is accounted by the term $\frac{\mu}{\rho C_p}\left(\frac{\partial u}{\partial y}\right)^2$, the joule

heating is accounted by the term $\frac{\sigma B_0^2 u^2}{\rho C_p}$due to the magnetic field, the value of heat generation/absorption per unit volume is accounted by the term $Q^* (T - T_\infty)$, where Q^* being an inflexible constant, the source term represents the heat generation when $Q^* > 0$ and the heat absorption when $Q^* < 0$.

Radiative heat flux [126] is:

$$q_r = -\frac{16\sigma^*}{3k^*} T_\infty^3 \frac{\partial T}{\partial y}, \tag{2.3.6}$$

The similarity variable is defined as $\eta = \sqrt{\frac{a}{\nu}} y$ and the stream function is defined as $\psi = \sqrt{a\nu}\, x f(\eta)$.
From η and ψ, we get

$$u = \frac{\partial \psi}{\partial y} = axf'(\eta), \quad v = -\frac{\partial \psi}{\partial x} = -\sqrt{a\nu} f(\eta), \quad \theta(\eta) = \frac{T - T_\infty}{T_w - T_\infty}, \tag{2.3.7}$$

Continuity equation (2.3.1) is satisfied. Equations (2.3.2) and (2.3.3) will reduced in the following form:

$$f''' + Gr_T \theta + ff'' - (f')^2 - Mf' = 0, \tag{2.3.8}$$

$$\left(1 + \frac{4}{3}Rd\right)\theta'' + Prf\theta' + Brf''f'' + MBrf'f' + Pr\beta\theta = 0, \tag{2.3.9}$$

with

$$f(\eta) = f_w, \; f'(\eta) = 1 + \gamma f''(\eta), \theta'(\eta) = -\lambda_1 (1 - \theta(\eta)), \text{ at } \eta = 0,$$
$$f'(\eta) \to 0, \; \theta(\eta) \to 0, \text{ as } \eta \to \infty, \tag{2.3.10}$$

where $Gr_T = \frac{g\beta_T (T_w - T_\infty)}{a^2 x}$, $M = \frac{\sigma B_0^2}{a\rho}$, $Pr = \frac{\mu C_p}{\kappa}$, $Rd = \frac{4\sigma^* T_\infty^3}{k^* \kappa}$, $f_w = -\frac{v_w}{\sqrt{a\nu}}$, $\gamma = l\sqrt{\frac{a}{\nu}}$, $Ec = \frac{U_w^2}{C_p (T_w - T_\infty)}$, $\beta = \frac{Q^*}{a\rho C_p}$, $\lambda_1 = \sqrt{\frac{\nu}{a}} \frac{h_{ft}}{\kappa}$, $Br = PrEc$.

Velocity gradient is $C_{fx} = \frac{\tau_w}{\rho U_w^2}$, where shear stress $\tau_w = \mu \left(\frac{\partial u}{\partial y}\right)_{y=0}$. Skin friction coefficient is $C_{fx} Re_x^{\frac{1}{2}} = f''(0)$.

Temperature gradient is $Nu_x = \frac{x q_w}{\kappa (T_w - T_\infty)}$, where $q_w = -\kappa \left(1 + \frac{16\sigma^* T_\infty^3}{3\kappa k^*}\right) \left(\frac{\partial T}{\partial y}\right)_{y=0}$ is heat flux at the wall. Nusselt number is $Nu_x Re_x^{-\frac{1}{2}} = -\left(1 + \frac{4}{3}Rd\right)\theta'(0)$, where local Reynold number $Re_x = \frac{x U_w}{\nu}$.

Generation of entropy is

$$S_G = \frac{\kappa}{T_\infty^2}\left(1+\frac{16\sigma^* T_\infty^3}{3\kappa k^*}\right)\left(\frac{\partial T}{\partial y}\right)^2 + \frac{\mu}{T_\infty}\left(\frac{\partial u}{\partial y}\right)^2 + \frac{\sigma B_0^2}{T_\infty}u^2, \tag{2.3.11}$$

we have entropy generation rate

$$N_G = \alpha_1\left(1+\frac{4}{3}Rd\right)\theta'^2 + Brf''^2 + MBrf'^2. \tag{2.3.12}$$

Bejan number is the proportion of heat and mass transfer entropy generation to total entropy generation.

$$Be = \frac{\alpha_1\left(1+\frac{4}{3}Rd\right)\theta'^2}{\alpha_1\left(1+\frac{4}{3}Rd\right)\theta'^2 + Brf''^2 + MBrf'^2} \tag{2.3.13}$$

where $N_G = \dfrac{T_\infty \nu S_G}{a\kappa(T_w - T_\infty)}$ denotes entropy generation rate, $\alpha_1 = \dfrac{T_w}{T_\infty} - 1$ is temperature difference parameter.

2.4 Solution by Homotopy Analysis Method

Homotopy method is a basic concept of topology. Liao [120] proposed HAM is used in Equations (2.3.8)-(2.3.9) with boundary conditions (2.3.10). Initial guesses $f_0(\eta)$, $\theta_0(\eta)$ and auxiliary linear operators $\mathcal{L}_f$, $\mathcal{L}_\theta$ for the HAM solution can be chosen as

$$f_0(\eta) = f_w + \frac{1}{1+\gamma}\left(1-e^{-\eta}\right), \theta_0(\eta) = \frac{\lambda_1}{1+\lambda_1}e^{-\eta}, \tag{2.4.1}$$

$$\mathcal{L}_f = \frac{\partial^3 f}{\partial \eta^3} - \frac{\partial f}{\partial \eta}, \mathcal{L}_\theta = \frac{\partial^2 \theta}{\partial \eta^2} + \frac{\partial \theta}{\partial \eta}, \tag{2.4.2}$$

with $\mathcal{L}_f\left(k_1 + k_2 e^{\eta} + k_3 e^{-\eta}\right) = 0$, $\mathcal{L}_\theta\left(k_4 + k_5 e^{-\eta}\right) = 0$, where $k_1, k_2, \ldots, k_5$ are arbitrary constants.

2.4.1 Zero-th order deformation

The following is the problem of zeroth order deformation:

$$\left.\begin{aligned}(1-q)\,\mathcal{L}_f\left[F(\eta;q) - f_0(\eta)\right] &= q\hbar_f \mathcal{N}_f\left[F(\eta;q)\right],\\ (1-q)\,\mathcal{L}_\theta\left[\Theta(\eta;q) - \theta_0(\eta)\right] &= q\hbar_\theta \mathcal{N}_\theta\left[\Theta(\eta;q)\right],\end{aligned}\right\} \tag{2.4.3}$$

The following is a list of nonlinear operators:

$$\mathcal{N}_f\left[F\left(\eta;q\right)\right]=\frac{\partial^3 F}{\partial\eta^3}+F\frac{\partial^2 F}{\partial\eta^2}-\left\{\frac{\partial F}{\partial\eta}\right\}^2-M\frac{\partial F}{\partial\eta}+Gr_T\Theta, \tag{2.4.4}$$

$$\mathcal{N}_\theta\left[\Theta\left(\eta;q\right)\right]=\left(1+\frac{4}{3}Rd\right)\frac{\partial^2\Theta}{\partial\eta^2}+PrF\frac{\partial\Theta}{\partial\eta}+Br\left(\frac{\partial^2 F}{\partial\eta^2}\right)^2+MBr\left(\frac{\partial F}{\partial\eta}\right)^2+Pr\beta\Theta, \tag{2.4.5}$$

Boundary conditions subject to:

$$F(0;q)=f_w,\ F'(0;q)=1+\gamma F''(0;q),\ \Theta'(0;q)=-\lambda_1(1-\Theta(0;q)), \tag{2.4.6}$$

$$F'(+\infty;q)=0,\ \Theta(+\infty;q)=0. \tag{2.4.7}$$

where F and Θ are unknown functions in terms of η and q, non-zero auxiliary parameters $\hbar_f$ and $\hbar_\theta$, non-linear operators $\mathcal{N}_f$ and $\mathcal{N}_\theta$. Furthermore where, embedding parameter $q\in(0,1)$.

$$F\left(\eta;0\right)=f_0\left(\eta\right),F\left(\eta;1\right)=f\left(\eta\right), \tag{2.4.8}$$

$$\Theta\left(\eta;0\right)=\theta_0\left(\eta\right),\Theta\left(\eta;1\right)=\theta\left(\eta\right). \tag{2.4.9}$$

If q varies from 0 to 1 then, F, Θ will be varies from $f_0\left(\eta\right)$, $\theta_0\left(\eta\right)$ to $f\left(\eta\right)$, $\theta\left(\eta\right)$. So one can obtain:

$$F\left(\eta;q\right)=f_0\left(\eta\right)+\sum_{i=1}^{\infty}f_i\left(\eta\right)q^i, \tag{2.4.10}$$

$$\Theta\left(\eta;q\right)=\theta_0\left(\eta\right)+\sum_{i=1}^{\infty}\theta_i\left(\eta\right)q^i, \tag{2.4.11}$$

where

$$f_i\left(\eta\right)=\left.\frac{1}{i!}\frac{\partial^i f(\eta;q)}{\partial\eta^i}\right|_{q=0},\ \theta_i\left(\eta\right)=\left.\frac{1}{i!}\frac{\partial^i\theta(\eta;q)}{\partial\eta^i}\right|_{q=0}, \tag{2.4.12}$$

here $\hbar_f$ and $\hbar_\theta$ are very important for the convergence of the series. If the non-zero auxiliary parameters are chosen in such a way that equations (2.4.10) and (2.4.11) converges at $q=1$. Thus, the following can be obtained:

$$f(\eta)=f_0\left(\eta\right)+\sum_{i=1}^{\infty}f_i\left(\eta\right), \tag{2.4.13}$$

$$\theta(\eta)=\theta_0\left(\eta\right)+\sum_{i=1}^{\infty}\theta_i\left(\eta\right), \tag{2.4.14}$$

2.4.2 i-th order deformation

The deformation equations in i^{th} order can be presented in the form

$$\mathcal{L}_f \left[f_i(\eta) - \chi_i f_{i-1}(\eta) \right] = \hbar_f \mathcal{R}_{f,i}(\eta), \tag{2.4.15}$$

$$\mathcal{L}_\theta \left[\theta_i(\eta) - \chi_i \theta_{i-1}(\eta) \right] = \hbar_\theta \mathcal{R}_{\theta,i}(\eta), \tag{2.4.16}$$

Under the conditions of the boundary

$$f_i(0) = 0, f_i'(0) = \gamma f_i''(0), \theta_i'(0) = \lambda_1 \theta_i(0), \ f_i'(+\infty) = 0, \theta_i(+\infty) = 0. \tag{2.4.17}$$

where,

$$\mathcal{R}_{f,i}(\eta) = f_{i-1}''' + \sum_{k=0}^{i-1} f_k f_{i-1-k}'' - \sum_{k=0}^{i-1} f_k' f_{i-1-k}' - M f_{i-1}' + G r_T \theta_{i-1} \tag{2.4.18}$$

$$\mathcal{R}_{\theta,i}(\eta) = \left(1 + \frac{4}{3} Rd\right) \theta_{i-1}'' + Pr \sum_{k=0}^{i-1} f_k \theta_{i-1-k}' + Br \sum_{k=0}^{i-1} f_k'' f_{i-1-k}'' + MBr \sum_{k=0}^{i-1} f_k' f_{i-1-k}' + Pr\beta\theta_{i-1}, \tag{2.4.19}$$

with

$$\chi_i = \begin{cases} 0, & i < 1 \\ 1, & i \geq 1 \end{cases} \tag{2.4.20}$$

The general solutions f_i, θ_i comprising the special solution f_i^*, θ_i^* are given by $f_i(\eta) = f_i^*(\eta) + k_1 + k_2 e^{\eta} + k_3 e^{-\eta}, \theta_i(\eta) = \theta_i^*(\eta) + k_4 + k_5 e^{-\eta}$. Here f_i^*, θ_i^* are given by the corresponding specific solutions i^{th}-order and constants equations k_j $(j = 1, 2, \ldots, 5)$ the boundary conditions shall be determined.

2.4.3 Convergence Analysis

For proper choice of $\hbar_f$ and $\hbar_\theta$, HAM solutions converges. The $f''(0)$ and $\theta'(0)$ functions are plotted to the appropriate approximations to get the allowable values of $\hbar_f$ and $\hbar_\theta$. From Fig. 2.2, we can choose $\hbar_f = -0.94$, $\hbar_\theta = -0.47$.

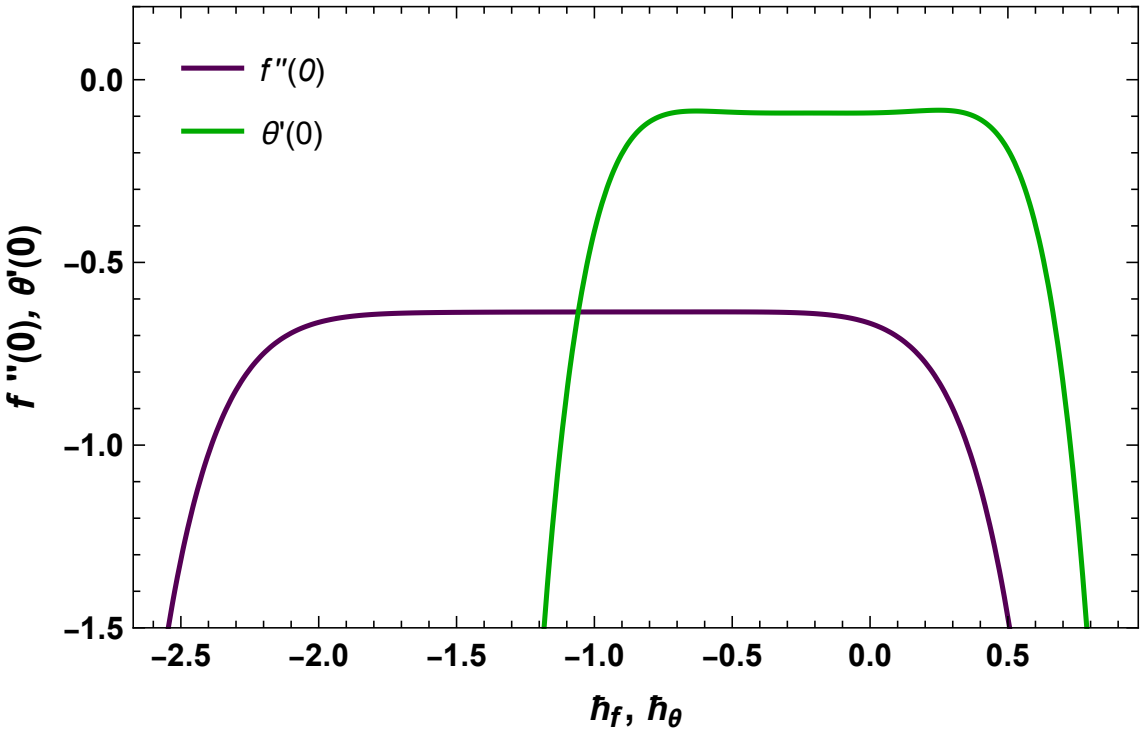

Figure 2.2: $\hbar$-curve for $f''(0),\ \theta'(0)$

2.5 Result and Discussion

The behavior of pertinent parameters on velocity, temperature, entropy rate and Bejan number are investigated in this section. The influence of M on the velocity profile $f'(\eta)$ is depicted in Figure 2.3. It has been demonstrated that enhancing the value of M results in a reduction in $f'(\eta)$. An upsurge in M produces a resistive type of force called Lorentz force in the flow, causing a decrement in $f'(\eta)$. The impact of f_w on $f'(\eta)$ is depicted in Figure 2.4. Based on this plot, we can conclude that $f'(\eta)$ declines as the f_w enhances. The result of γ on $f'(\eta)$ is demonstrated in Figure 2.5. The $f'(\eta)$ declined as the value of γ risen. This could be because stretching velocity is partially transforming the disturbance frictional retardation between the surface and the liquid's particles, causing a drop in fluid velocity. $f'(\eta)$ for rising values of Gr_T is revealed in Figure 2.6. $f'(\eta)$ is a growing function of Gr_T. The behaviour of Br on temperature profile $\theta(\eta)$ is evidenced in Figure 2.7. Clearly, a larger approximation of Br equates to a slower thermal conduction prompted by viscous dissipation, and as a result, temperature rises. The impact of M on temperature profile $\theta(\eta)$ is demonstrated in Figure 2.8. It has been witnessed that an upsurge in M raises the temperature. Some extra heat will be produced in the

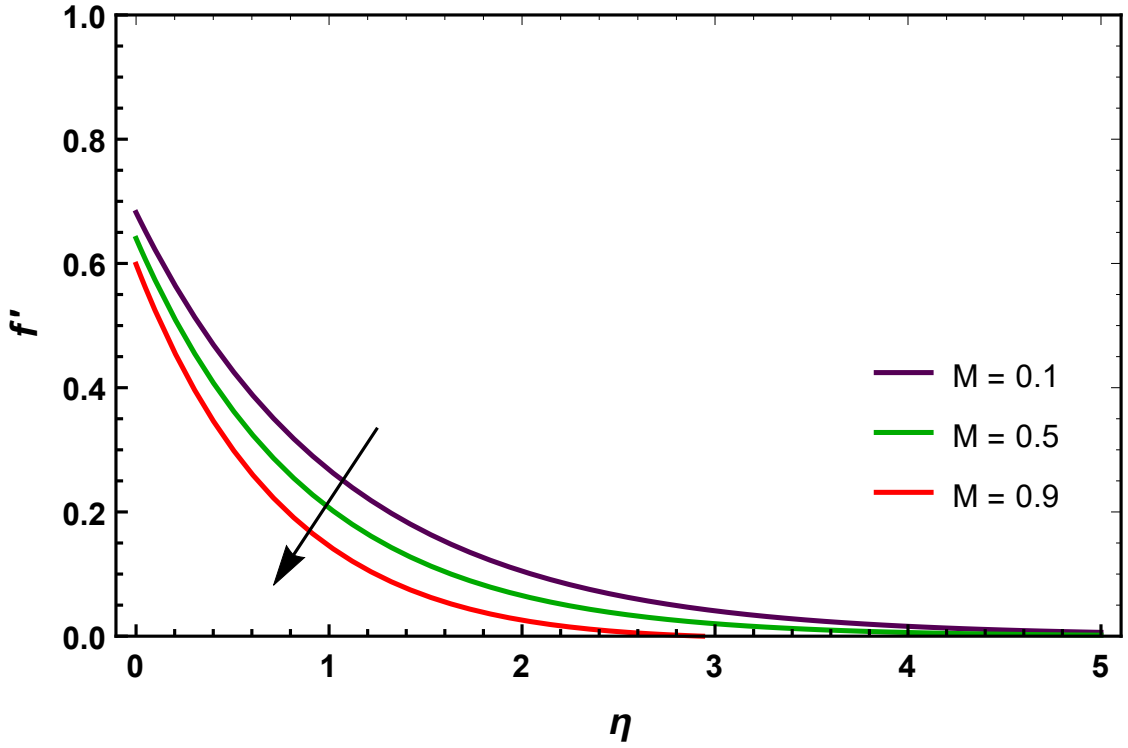

Figure 2.3: $f'(\eta)$ via M

flow as an outcome of the Lorentz force. As exhibited in Figure 2.9, boosting the value of Pr, lowers the rate of heat transfer in fluid significantly because of enhancing values of Pr decreases the rate of thermal diffusivity. The impact of Rd on $\theta(\eta)$ is illustrated in Figure 2.10. The figure evidently demonstrates that expanding Rd tends to increase temperature. Enhanced Rd liberates heat energy to the flow, which assist in appreciating the temperature field.

Figures 2.11 and 2.12 show how N_G and Be are related to Br. Thermal conduction declines so N_G raises, for larger approximations of Br. However, Be declines against Br. The effect of M on N_G and Be is depicted in Figures 2.13 and 2.14. As M rises, Lorentz force raises, enabling more disturbance to the fluid flow and thus growing $\mathcal{N}_G$. When compared to larger values of M, N_G and Be is boosted. Figures 2.15 and 2.16 show how N_G and Be are related to α_1, respectively. Physically, as α_1 increases, N_G and Be increases. Numerical outcomes of N_G and Be via pertinent parameters can be found in Table 2.1 and Table 2.2.

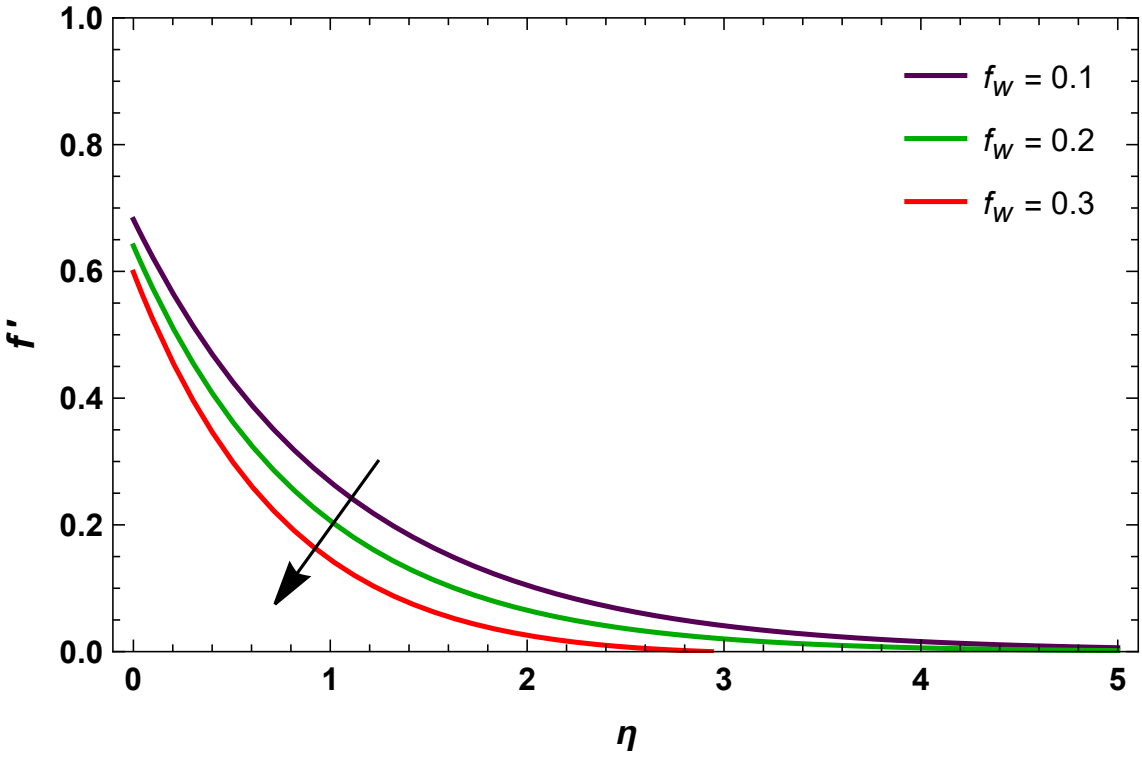

Figure 2.4: $f'(\eta)$ via f_w

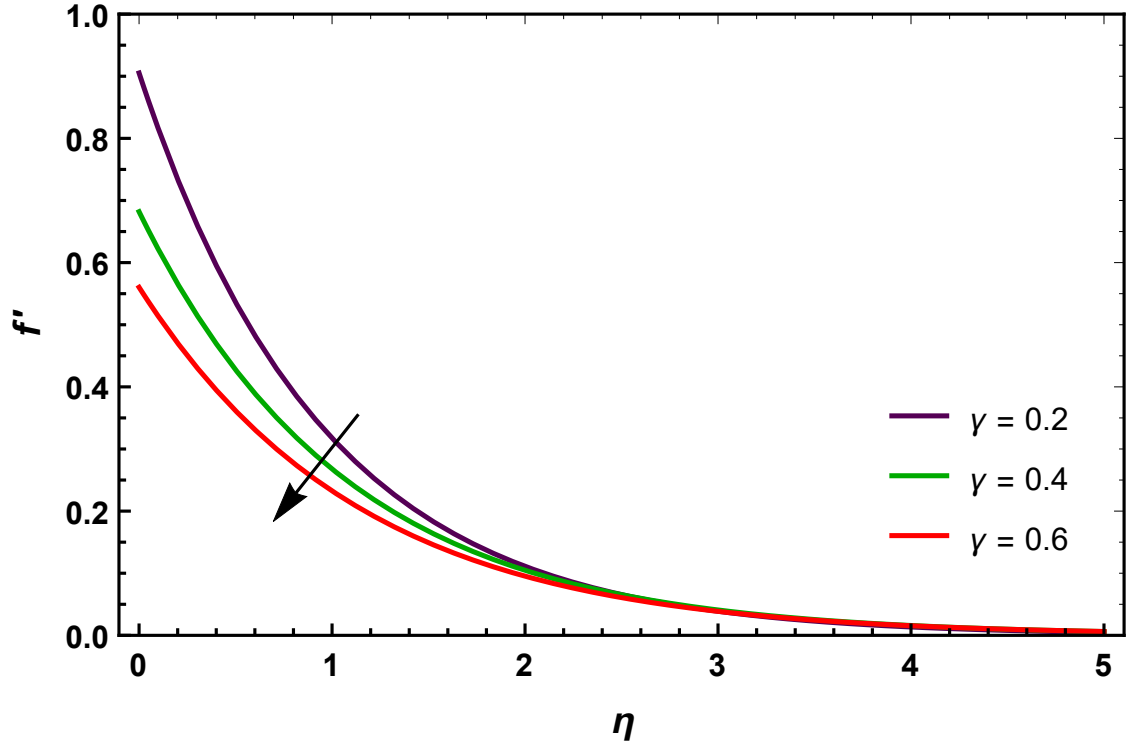

Figure 2.5: $f'(\eta)$ via γ

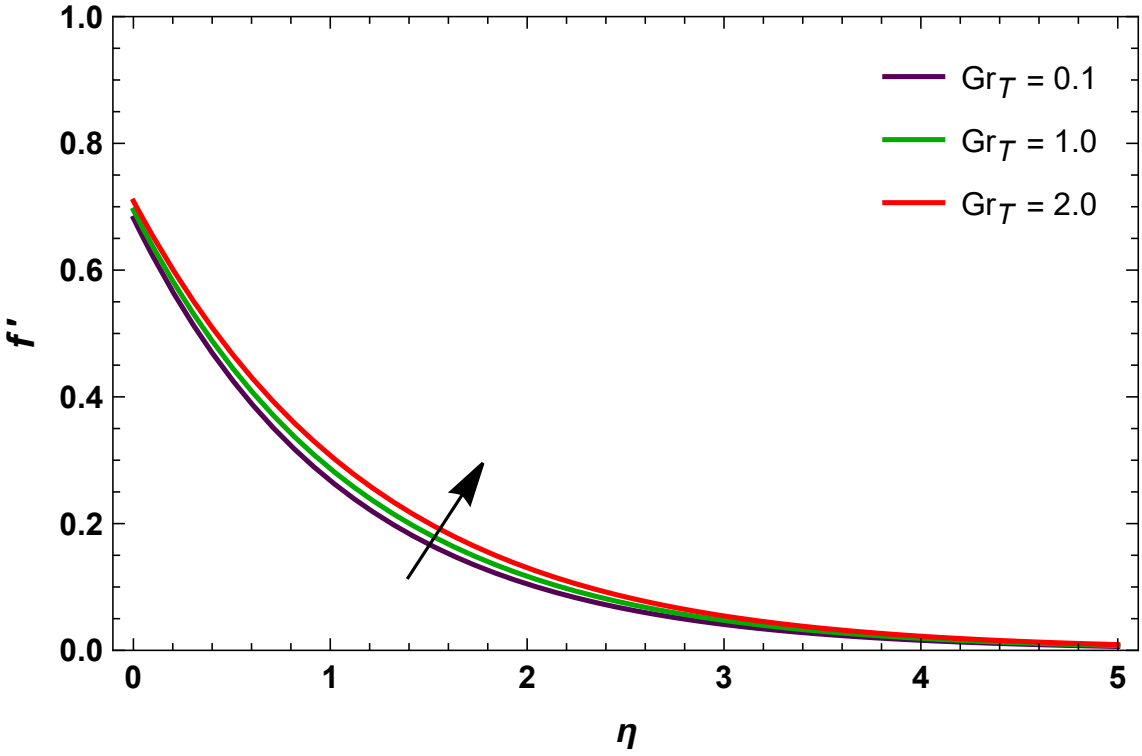

Figure 2.6: $f'(\eta)$ via Gr_T

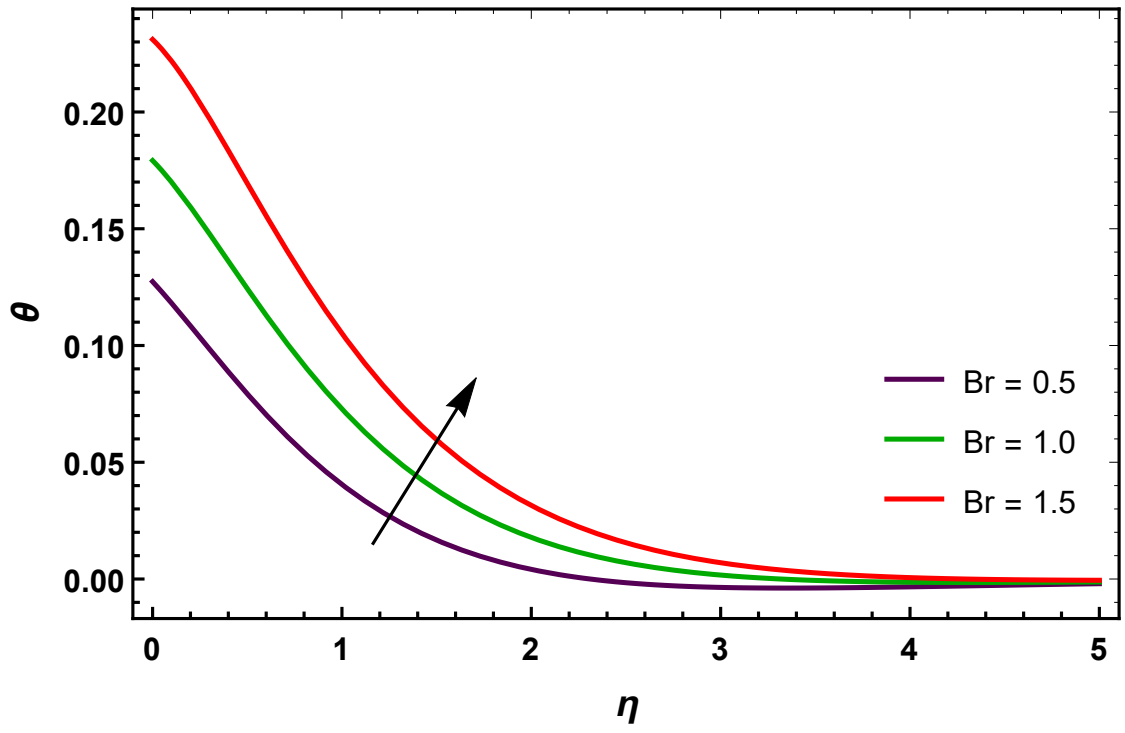

Figure 2.7: $\theta(\eta)$ via Br

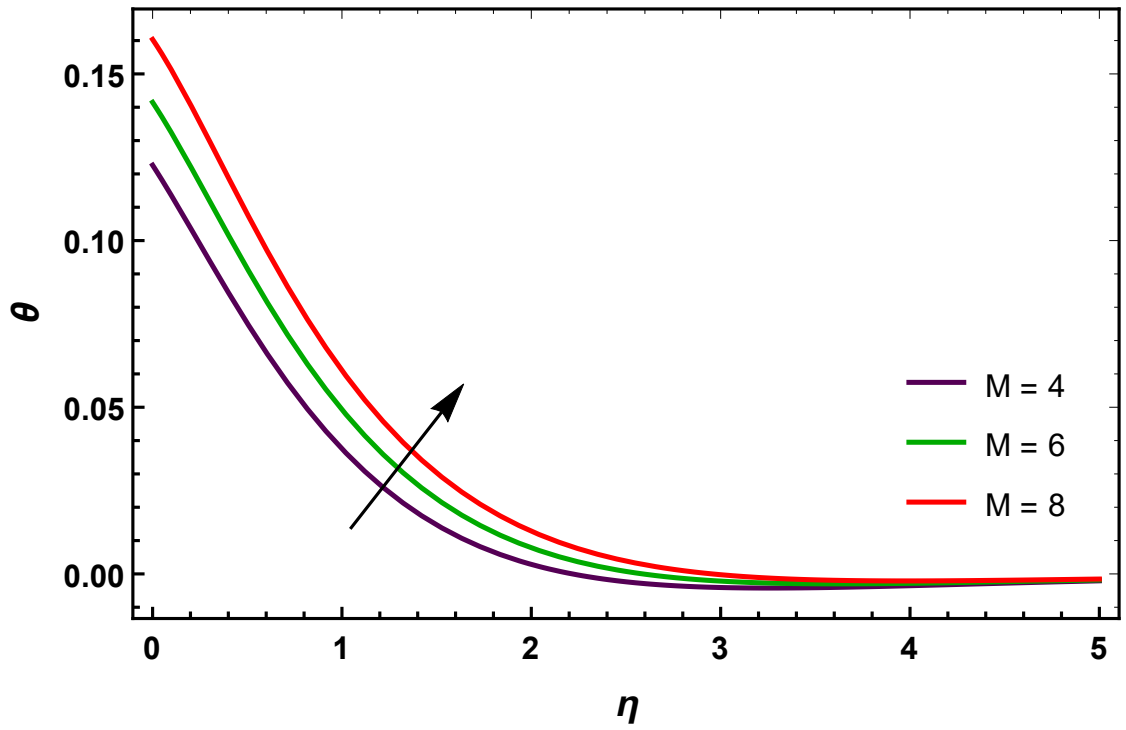

Figure 2.8: $\theta(\eta)$ via M

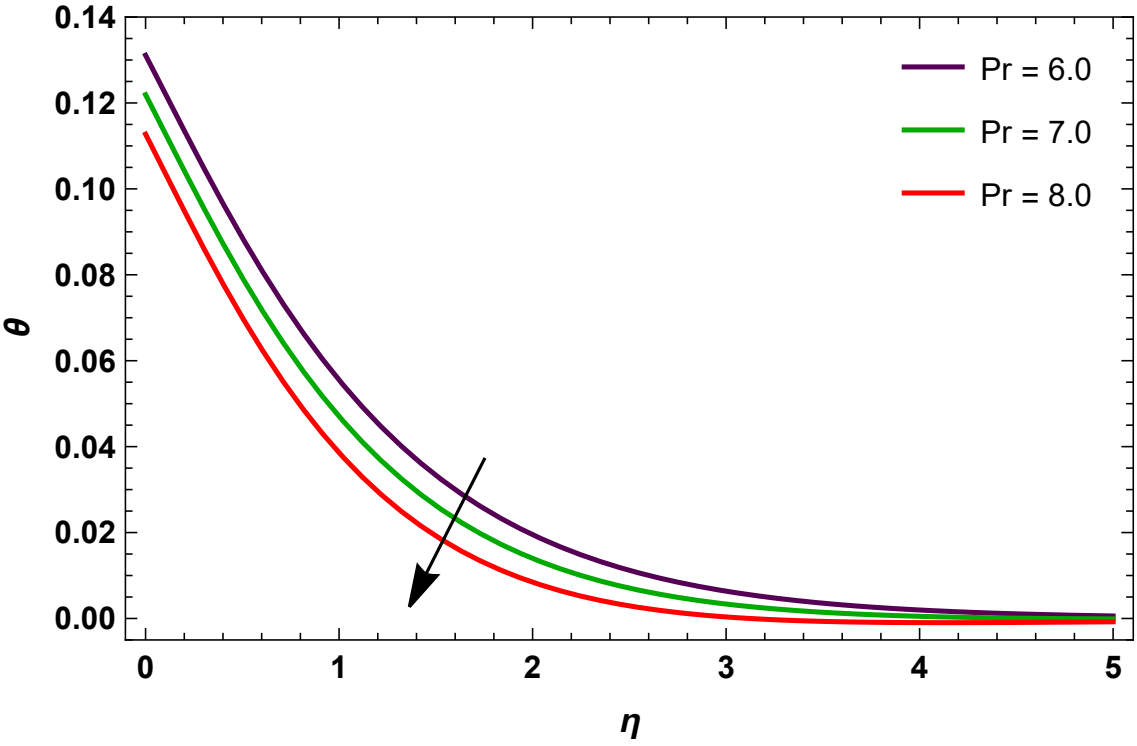

Figure 2.9: $\theta(\eta)$ via Pr

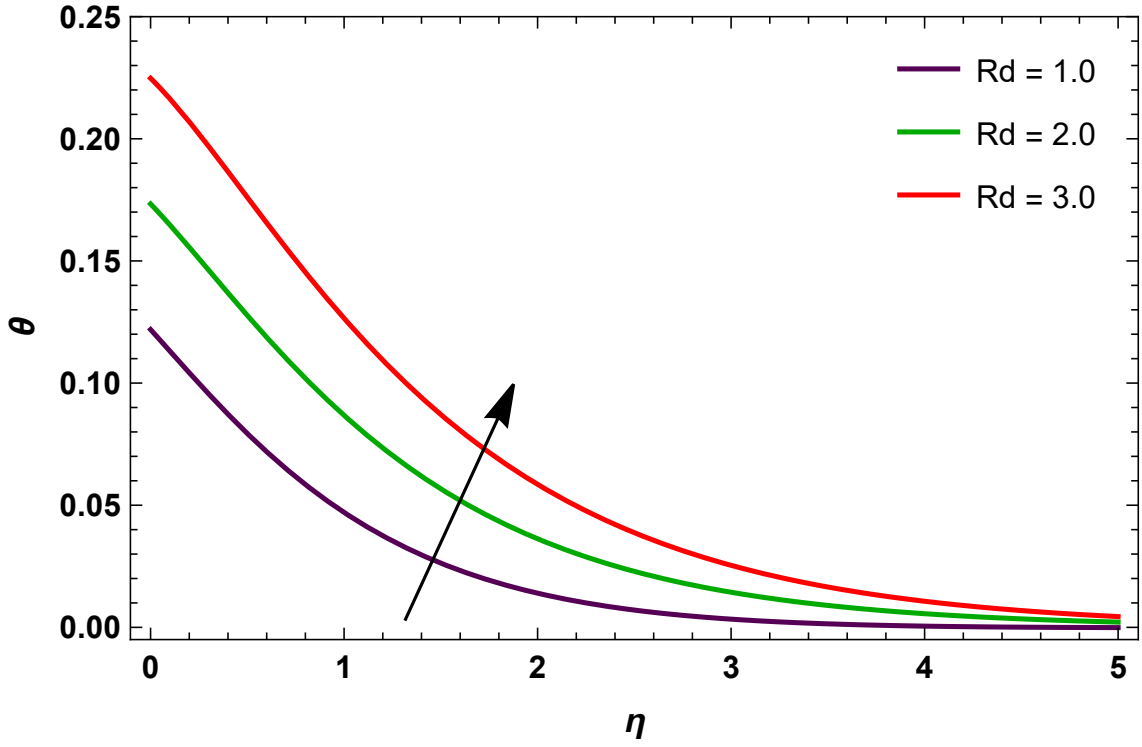

Figure 2.10: $\theta(\eta)$ via Rd

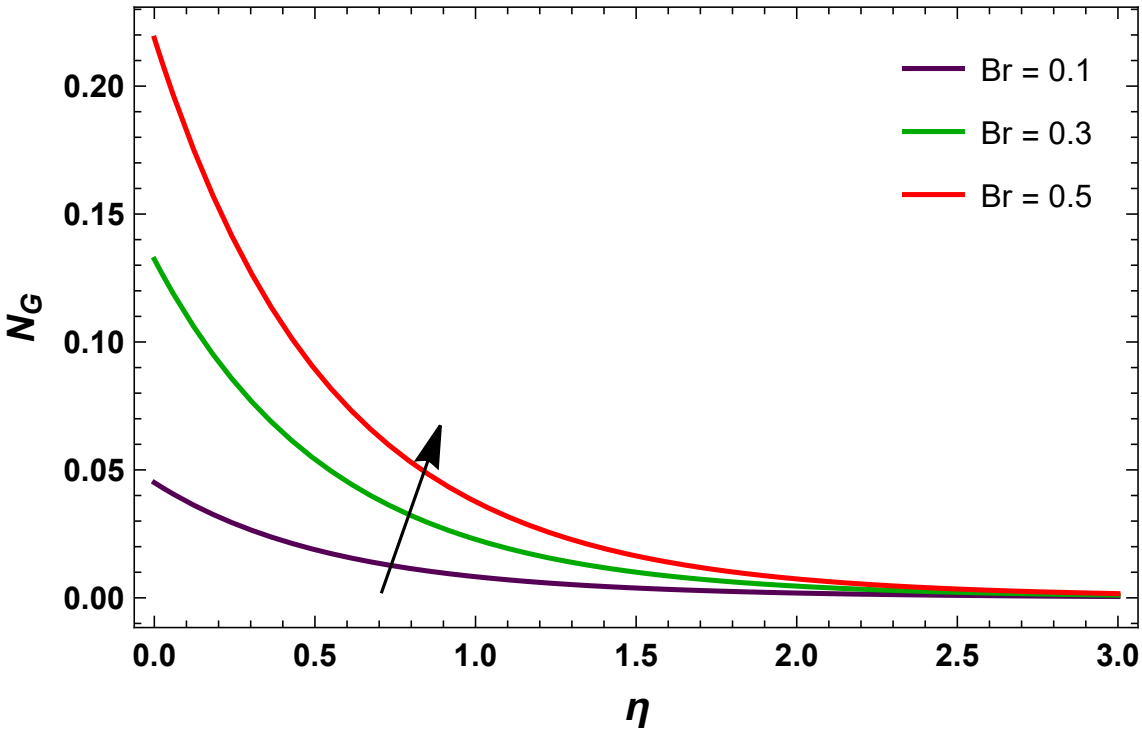

Figure 2.11: $\mathcal{N}_G$ via Br

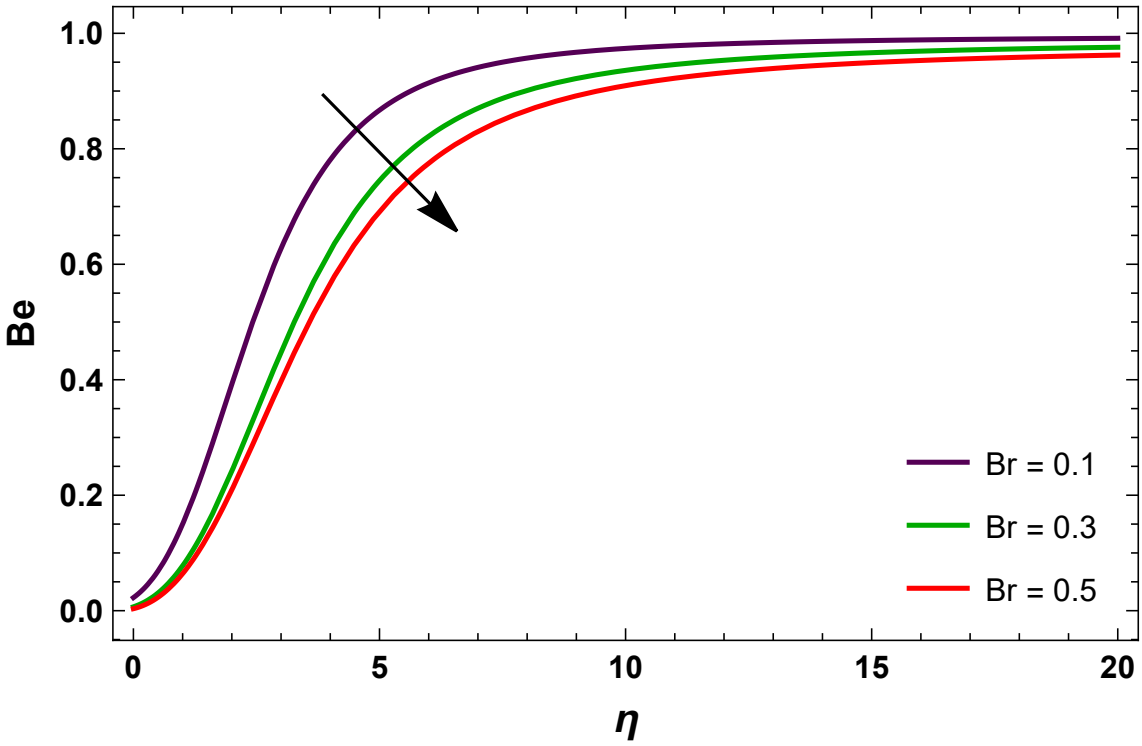

Figure 2.12: Be via Br

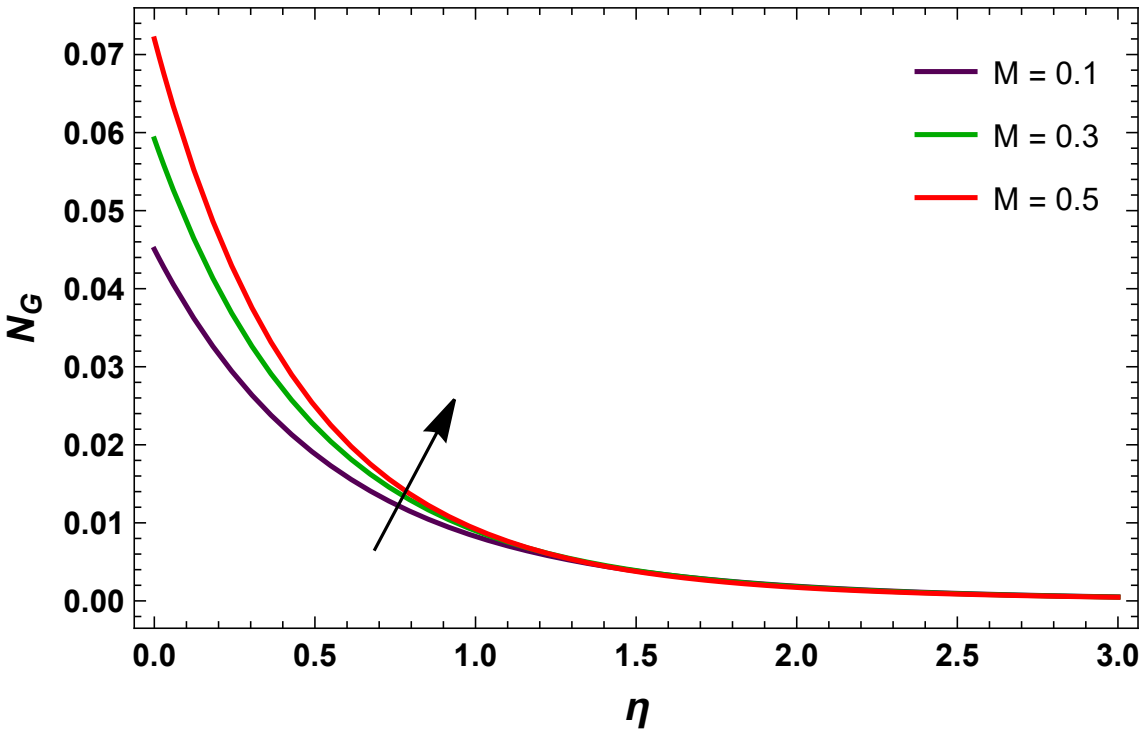

Figure 2.13: $\mathcal{N}_G$ via M

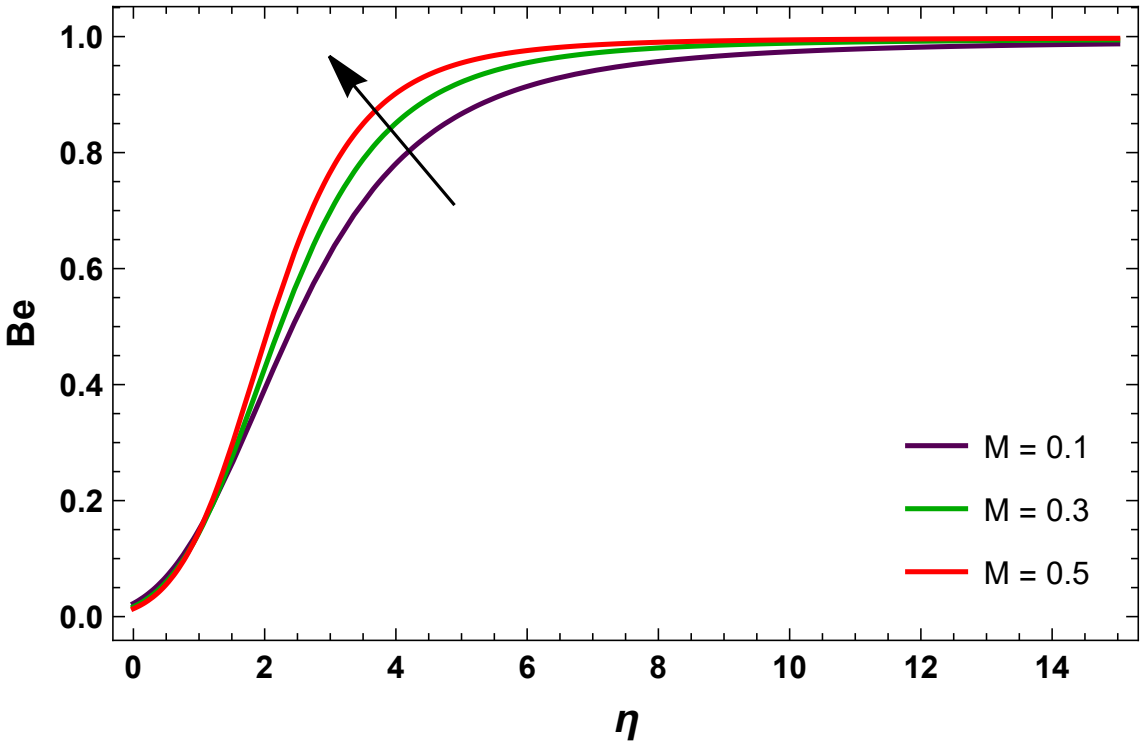

Figure 2.14: Be via M

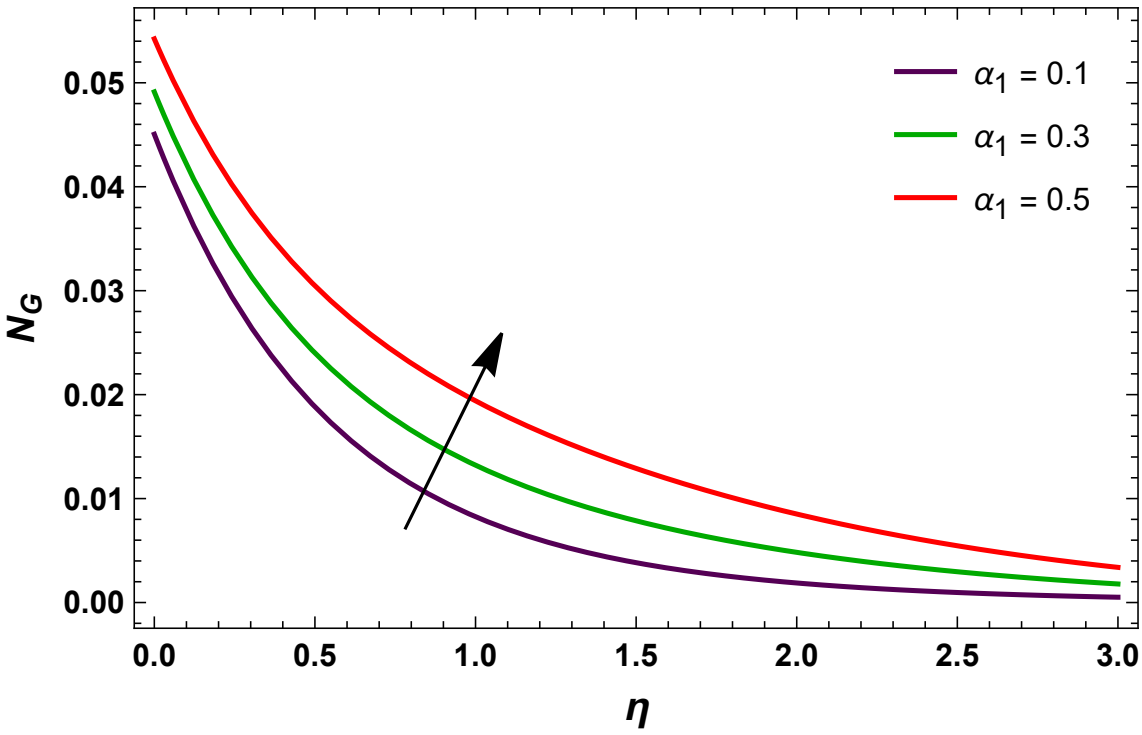

Figure 2.15: $\mathcal{N}_G$ via α_1

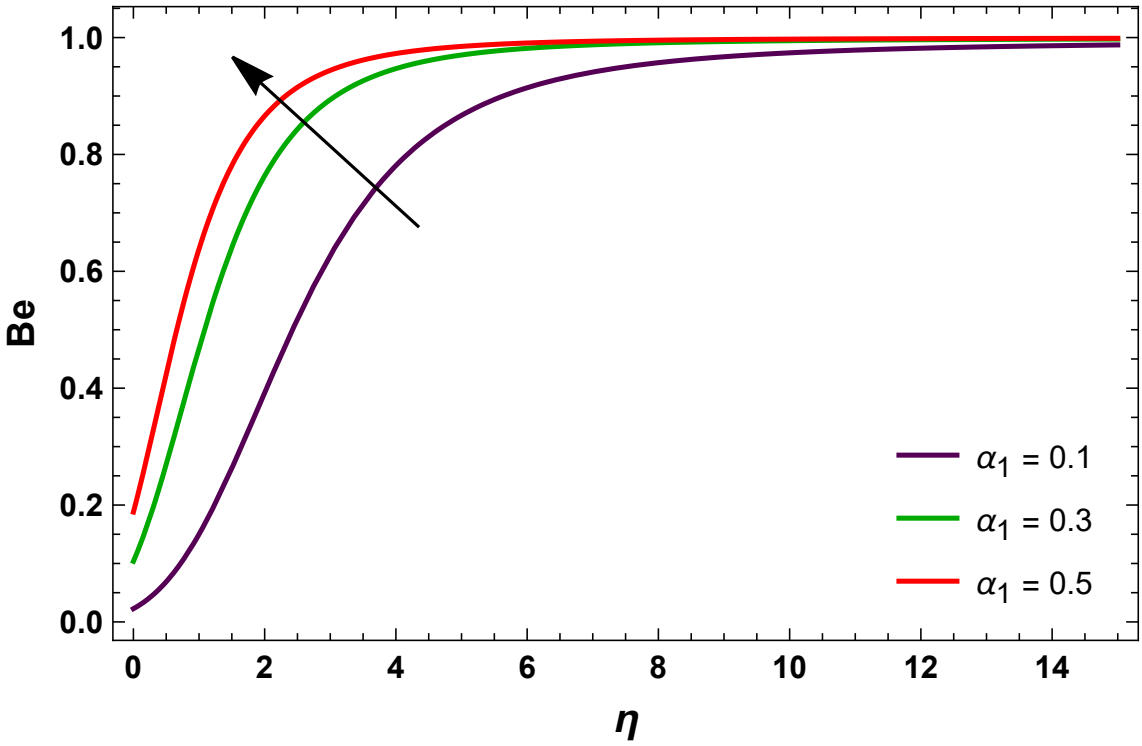

Figure 2.16: Be via α_1

Table 2.1: Numerical outcomes of N_G via Br, M, Rd and α_1.

Br	M	Rd	α_1	N_G for $Pr = 0.7$, $\eta = 0$	N_G for $Pr = 7.0$, $\eta = 0$
0.1	0.1	0.7	0.1	0.045048	0.046602
0.2				0.088791	0.091538
0.3				0.132321	0.136413
	0.2			0.052313	0.053812
	0.3			0.059197	0.060643
		0.8		0.045022	0.046681
		0.9		0.044992	0.046758
			0.2	0.046068	0.048181
			0.3	0.047087	0.049758

Table 2.2: Numerical outcomes of Be via Br, M, Rd and α_1.

Br	M	Rd	α_1	Be for $Pr = 0.7$, $\eta = 0$	Be for $Pr = 7.0$, $\eta = 0$
0.1	0.1	0.7	0.1	0.035034	0.033866
0.2				0.017496	0.016971
0.3				0.011554	0.011208
	0.2			0.030041	0.029204
	0.3			0.026456	0.025826
		0.8		0.037274	0.035950
		0.9		0.039493	0.038002
			0.2	0.068519	0.065515
			0.3	0.100550	0.095156

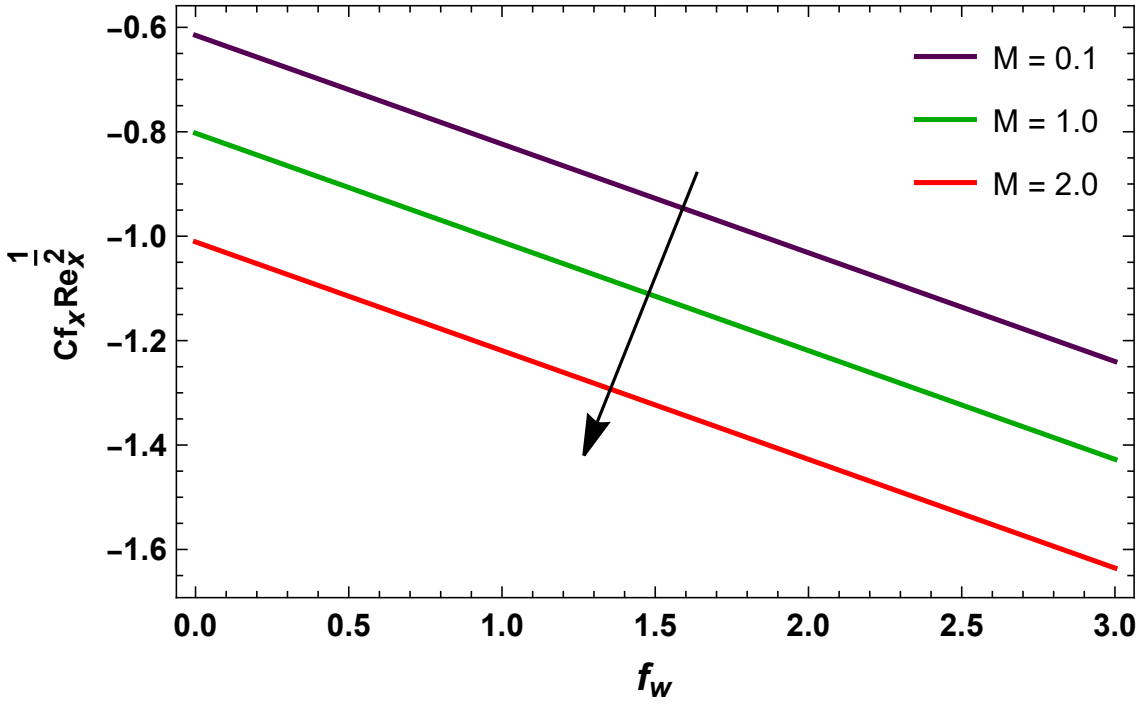

Figure 2.17: $C_{fx}Re_x^{1/2}$ via M

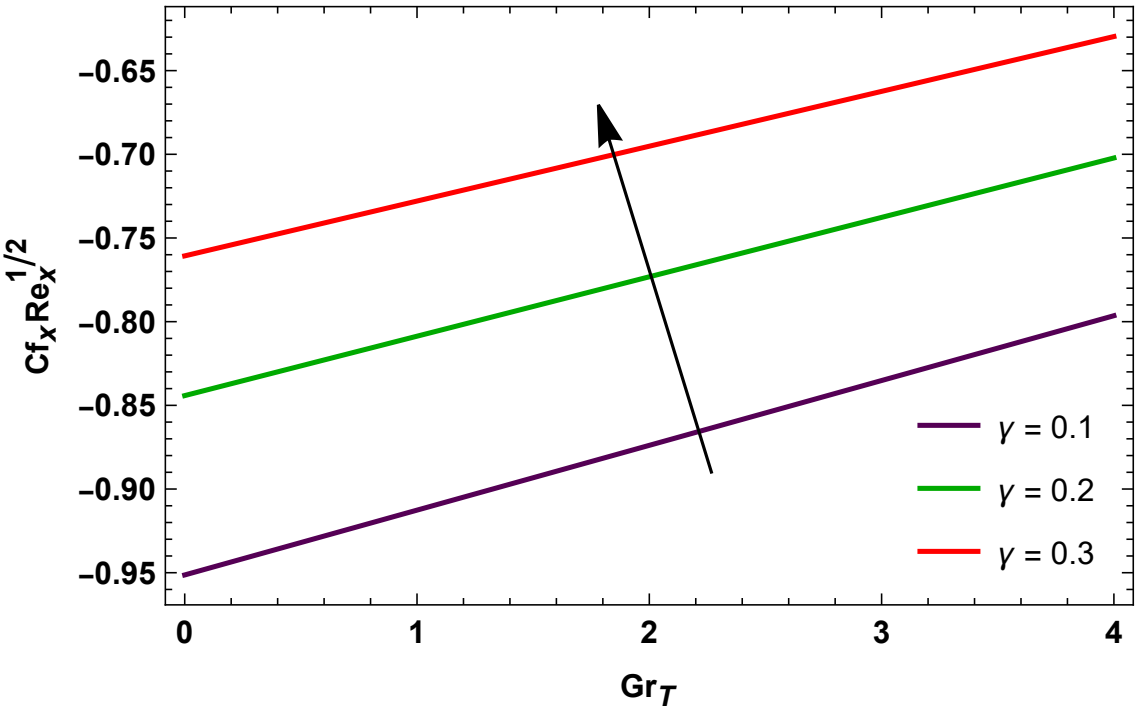

Figure 2.18: $C_{fx}Re_x^{1/2}$ via γ

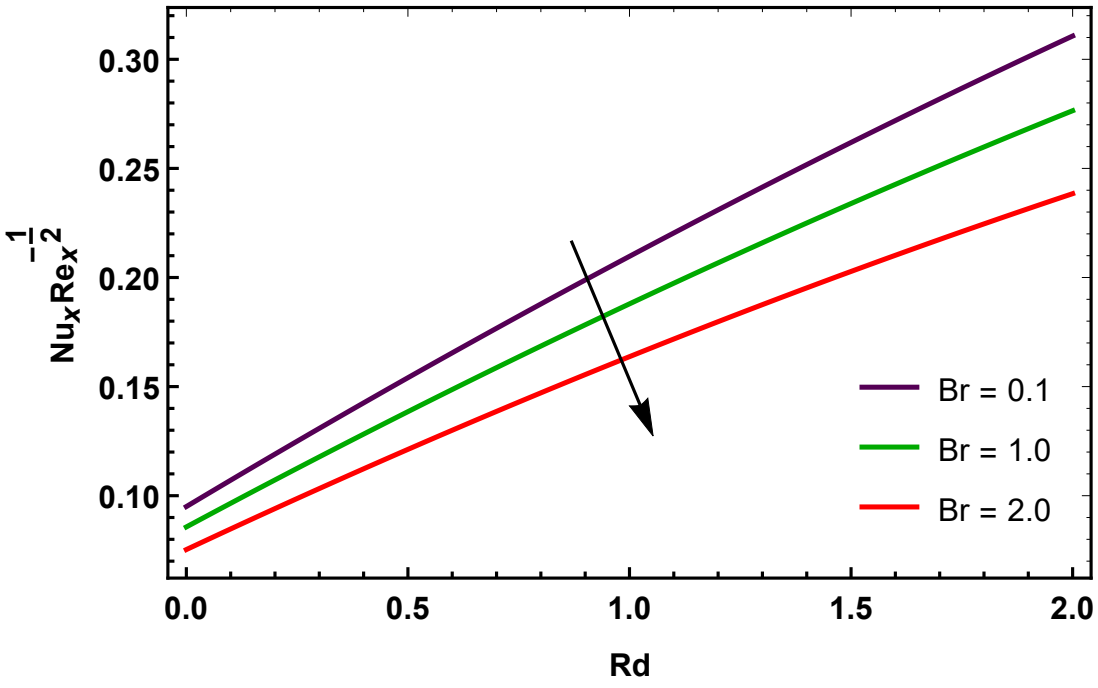

Figure 2.19: $Nu_x Re_x^{-1/2}$ via Br

Table 2.3: Numerical outcomes of $C_{fx}Re_x^{1/2}$ via f_w, M, γ and Gr_T.

f_w	M	γ	Gr_T	$C_{fx}Re_x^{1/2}$
0.1	0.1	0.5	0.1	-0.63512
0.2				-0.65837
0.3				-0.68195
	0.2			-0.65748
	0.3			-0.67822
		0.6		-0.58835
		0.7		-0.54851
			0.2	-0.63293
			0.3	-0.63075

Table 2.4: Numerical outcomes of $Nu_xRe_x^{-1/2}$ via λ_1, M, Br, Pr, β and Rd.

λ_1	M	Br	Pr	β	Rd	$Nu_xRe_x^{-1/2}$
0.1	0.1	0.1	7.0	0.1	0.7	0.17712
0.2						0.32935
0.3						0.46184
	0.2					0.17628
	0.3					0.17548
		0.2				0.17568
		0.3				0.17424
			8.0			0.17833
			9.0			0.17867
			0.7			0.14948
			0.8			0.15019
			0.9			0.15089
				0.2		0.17394
				0.3		0.16424
					0.8	0.18858
					0.9	0.19996

Figures 2.17 and 2.18 demonstrate that Skin friction increases for γ and Gr_T while decreases for f_w and M. Also Numerical outcome of Skin friction gives same

characteristics for γ, M, f_w and Gr_T through Table 2.3. Figure 2.19 shows that Nusselt number reduces for Br while increases for Rd. Table 2.4 shows the numerical outcome of Nusselt number for different values of λ_1, M, Br, Pr, β and Rd. Nusselt number enhances for large amount of Rd, λ_1 and Pr, while behaves opposite for Br, β, and M.

2.6 Conclusion

Current paper presents joule heating, heat generation/absorption and viscous dissipation on 2D laminar MHD fluid flow passing over vertical stretching surface. Physical behavior of entropy optimization rate examined in this research. Cartesian coordiantes system is used to model the flow equations. Using similarity variables, system of PDEs converted into system of ODEs. The problem is solved using HAM. The main findings are:

- M, γ and f_w have similar characteristics for velocity profile.
- Velocity is enhanced against rising amount of Gr_T.
- Rd, M and Br have similar characteristics for temperature profile.
- Temperature is diminished via Pr.
- M, α_1 and Br have similar characteristics for N_G.
- Bejan number has increment for large amount of α_1 and M while decreases for higher values of Br.
- Skin friction coefficient is enhanced via γ and Gr_T and declined via M and f_w.
- Nusselt number is declined against rising values of Br, β and M while behaves opposite for λ_1, Pr and Rd.
- N_G is enhanced via Br, M and α_1 while declined via Rd. Whereas Be is increased via Rd and α_1 while decreased via Br and M, also compared for different values of Pr through tables.